

# Raman Scattering and X-Ray-Scattering Studies on $\text{KBr}_{1-x}\text{I}_x$ , $\text{KCl}_{1-x}\text{I}_x$ , and $\text{K}_{1-x}\text{Rb}_x\text{Cl}$ <sup>†</sup>

Indira R. Nair\* and Charles T. Walker‡

*Department of Physics, Northwestern University, Evanston, Illinois 60201*

(Received 31 August 1972)

Raman-scattering and x-ray-scattering experiments have been performed on the mixed-alkali-halide systems  $\text{KBr}_{1-x}\text{I}_x$ ,  $\text{KCl}_{1-x}\text{I}_x$ , and  $\text{K}_{1-x}\text{Rb}_x\text{Cl}$ , and the results have been compared with our earlier work on the  $\text{KCl}_{1-x}\text{Br}_x$  system. Both powder-pattern and line-broadening studies have been carried out using x-ray scattering. Our earlier work on  $\text{KCl}_{1-x}\text{Br}_x$  has been reevaluated and the previous lower limit of a few hundred angstroms for cluster sizes has been raised to 4000 Å. The  $\text{KBr}_{1-x}\text{I}_x$  system has been seen to display several different microscopic structures. For  $x > 0.7$  the bulk crystals were seen to have the x-ray properties of bulk crystals. For  $x < 0.1$ , the bulk crystals were seen to be composed of crystallites a few hundred angstroms in size. For  $0.7 \geq x \geq 0.1$ , the bulk crystals were found to consist of three distinct phases, occurring in crystallites ranging in size from 300 to 1650 Å. Raman spectra for  $\text{KBr}_{1-x}\text{I}_x$  in the ranges  $x < 0.1$  and  $x > 0.7$  and for  $\text{KCl}_{1-x}\text{I}_x$  were seen to be of  $A_{1g}$  and  $T_{2g}$  symmetry and showed the same systematic behavior as the  $\text{KCl}_{1-x}\text{Br}_x$  system reported earlier. That is, certain spectral features could apparently be identified with particular zone-boundary phonons of the mixed crystal and the variation of frequency of these phonons as a function of concentration  $x$  could be studied. The variation was seen to be linear. Similar results were seen to pertain for  $\text{K}_{1-x}\text{Rb}_x\text{Cl}$ , except that the mixed-crystal spectra were of  $E_g$  and  $T_{2g}$  symmetry. However, it is also suggested that the Raman results may merely be a reflection of the fact that the zone-boundary phonons observed also happen to correspond to the peaks in the phonon density of states.

## I. INTRODUCTION

This paper reports the study of the mixed-alkali-halide systems  $\text{KBr}_{1-x}\text{I}_x$  and  $\text{K}_{1-x}\text{Rb}_x\text{Cl}$  throughout the entire composition range, and of  $\text{KCl}_{1-x}\text{I}_x$  for a single composition, using Raman scattering and x-ray scattering. The corresponding study of  $\text{KCl}_{1-x}\text{Br}_x$  has been published before,<sup>1</sup> and where necessary some of the results are repeated here to facilitate the comparison of the systems.

The selection rules arising from translational and inversion symmetry for Raman scattering from phonons in crystals are well known.<sup>2</sup> Translational symmetry leads to the possibility of identification of phonon quasimomentum and wave vector. Conservation of momentum then implies that only phonons with wave vector  $q \approx 0$ , i. e., near the center of the Brillouin zone, participate in Raman scattering of light in the visible region. Inversion symmetry has the following consequences: A crystal in which every lattice point is at a center of inversion symmetry cannot have a nonvanishing third-order tensor property and thus cannot cause first-order Raman scattering due to an electro-optic type of mechanism. If, on the other hand, inversion symmetry is just one of the symmetry operations of the crystal, then only phonons of even parity, with respect to the center of inversion, can scatter in first order, again assuming an electro-optic mechanism and with the incident light in a nonresonant region of energy. Consequently, pure

alkali halides do not scatter light in first order and have only second-order spectra arising from two-phonon combinations, such that the net change in wave vector is close to zero.

When a substitutional impurity is introduced, inversion symmetry and translational symmetry are broken. Loss of translational symmetry means that momentum conservation no longer implies the  $q \approx 0$  quasimomentum selection rule. Thus phonons of allowed symmetry all over the Brillouin zone can now be observed in Raman scattering, if the cross section is large enough. In a crystal of low impurity concentration, the impurity is still at a center of inversion but its neighbors are not. Thus first-order Raman scattering becomes allowed, and those phonons whose parity is even with respect to the impurity can now be observed in a first-order spectrum, again provided the electron-phonon coupling, which is the intermediate mechanism in electro-optic Raman scattering by phonons, is strong enough to give observable intensities.

The phonons which are Raman active in this case are those whose displacement patterns are such that the impurity does not move, as only these will be even with respect to the impurity. If the impurity is isotopic in behavior, then the induced first-order Raman spectrum can yield information about the phonon spectrum. In particular, this frequency spectrum is expected to reflect the one-phonon density of states, as this is the most strongly frequency-dependent term in the cross

section.<sup>3</sup> This was first observed in  $Tl^+$ -doped alkali halides by Harley, Page, and Walker<sup>4</sup> and in  $KBr:Cl$  by Hurrell, Porto, Damen, and Mascarenhas.<sup>5</sup>

As the impurity concentration is increased, a mixed crystal with a new characteristic frequency spectrum, no longer derivable from the pure crystal eigenfunctions by perturbation theory, would be obtained. Thus, Raman spectra in mixed crystals allow study of the evolution of phonon spectra as one moves from one end member of a mixed system to the other.

## II. MIXED ALKALI HALIDES

### A. Systematics of Mixed Alkali Halides

The phase diagrams, lattice-parameter variation, and thermodynamic parameters of mixed alkali halides have been investigated extensively. The most detailed of these studies were made by Matsen and Beach,<sup>6</sup> by Tobolsky,<sup>7</sup> and by Ahtee.<sup>8</sup> From the results of his x-ray studies, Tobolsky concluded that two alkali halides  $AB$  and  $AC$  will form continuous solid solutions  $AB_{1-x}C_x$  ( $0 < x < 1$ ) at 20 °C, provided the difference  $\delta$  between their lattice parameters is less than 6%.

At this point it is worth describing what is meant by a "continuous solid solution"—or by a "mixed crystal" in the jargon of physics. Two compounds or elements are said to form a continuous solid solution if a single lattice parameter, as measured by x-ray-powder photographs, can be assigned to the solid solution at all compositions. The fact that a Debye-Scherrer photograph yields a single lattice parameter for a solid solution indicates that the displacement of ions due to local change in coordination is perfectly random. This again means that, on an "average," i. e., in a measurement such as the Debye-Scherrer measurement where many unit cells are simultaneously sampled, one has translational symmetry. It is necessary to distinguish this definition—usually used by the x-ray crystallographer—of translational symmetry from the more stringent condition of translational symmetry required when discussing selection rules. Thus the local loss of translational symmetry caused by the substitution of the ion  $C$  for  $B$  in  $AB_{1-x}C_x$  modifies the selection rules in a process such as Raman scattering, whereas to the x-ray crystallographer the system is still "periodic" and hence has over-all translational symmetry.

Wasastjerna<sup>9</sup> and Luova<sup>10</sup> studied diffuse x-ray scattering from pure alkali halides and from equimolar  $KCl-KBr$  and  $KCl-RbCl$  and found an average static shift of 0.14 Å of the cation and 0.09 Å of the anion. Although Wasastjerna concluded that a certain long-range order existed in mixed alkali halides, Luova's more detailed work showed that no long-range order exists, and that the measured

TABLE I. Parameters of mixed-alkali-halide systems of interest.

Systems	$\delta$	$T_c$ (K) <sup>a</sup>		Max. % deviation <sup>b</sup> from		Miscibility limits at 300 K
		Theory	Experiment	Vegard's law	Rutger's law	
$K_{1-x}Rb_xCl$	4.5	195		0.09	0.08	completely miscible
$KCl_{1-x}Br_x$	4.8	200	<180	0.08	0.03	completely miscible
$KCl_{1-x}I_x$	12.3		melting point			$0.05 < x < 0.9$
$KBr_{1-x}I_x$	7.1	370	>478	0.12	0.02	$0.1 < x < 0.8$ dependent on moisture

<sup>a</sup>Reference 11.

<sup>b</sup>Reference 8.

local displacements are scattered randomly in direction through the lattice, resulting in the possibility of definition of a single lattice parameter from a Debye-Scherrer photograph. Durham and Hawkins<sup>11</sup> have considered the possible coordinate ion schemes which lower the site symmetries of the common ion  $A$  in the mixed system  $AB_{1-x}C_x$  and calculated the probability of a given configuration for certain values of  $x$ , assuming a random solid solution. If any kind of order were to exist, so that the predominantly polarizable ion had a preferred site symmetry, this should be also evidenced in the first-order Raman spectrum by a change of the form of the scattering tensors.

The relevant parameters of the systems of interest obtained from the x-ray studies referred to are summarized in Table I. The table shows that even systems which are single phase at room temperature have theoretically estimated critical temperatures  $T_c$  (below which there should appear a miscibility gap in the systems) above liquid-nitrogen temperature. However, no segregation has been observed at low temperature because of the extremely low values of diffusion coefficients at these temperatures.

The phase diagram of the  $KBr-KI$  system below 300 °C has been studied by Luova and Tannila<sup>12</sup> and the solidus-liquidus curved by Luova and Muurinen.<sup>13</sup> This is the only system studied in the present work that has a miscibility gap at room temperature. This miscibility gap is dependent on the moisture present and thus different values have been reported by different workers. Even in these studies, however, the time required to reach the equilibrium configuration has not been determined. The miscibility limits observed in the present work are discussed later.

In the continuous solid solutions of alkali halides, Retgers's law<sup>14</sup> (additivity of molar volumes) and Vegard's law<sup>15</sup> (linear variation of lattice parameter with composition) are closely followed, as indicated by x-ray studies. The fact that the random

substitution of ions in the lattice gives rise to coherent x-ray-diffraction patterns, as discussed before, justifies the use of concepts of site symmetry and of Brillouin zone in the case of mixed crystals.

### B. Phonons in Mixed Crystals

Most of the studies of phonons in mixed crystals have made use of infrared or Raman spectroscopy. The only neutron study of a mixed alkali halide over a wide range of concentration has been that of Buyers and Cowley<sup>16</sup> on the KBr-RbBr system. The infrared measurements allow observation only of the behavior of the  $q = 0$  phonons. Based on the infrared and Raman experiments, two types of behavior can be identified for the  $q = 0$  phonons in mixed crystals.<sup>17</sup> In one class, the phonon frequency (of each of the modes, infrared or Raman active or both) varies continuously from the frequency characteristic of one end member to that of the other, the strength of the mode varying according to the polarizability of the ion being added. This, defined as "one-mode behavior," has been observed in  $\text{Na}_{1-x}\text{K}_x\text{Cl}$ ,  $\text{Ni}_{1-x}\text{Co}_x\text{O}$ ,  $\text{K}_{1-x}\text{Rb}_x\text{Cl}$ ,  $\text{GaAs}_{1-x}\text{Sb}_x$ ,  $\text{Zn}_{1-x}\text{Cd}_x\text{S}$ , and  $\text{ZnSe}_{1-x}\text{Te}_x$  by infrared reflectivity and transmission experiments,<sup>18</sup> and in  $(\text{Ca}, \text{Ba})_{1-x}\text{Sr}_x\text{F}_2$ ,<sup>19</sup> and  $\text{KCl}_{1-x}\text{Br}_x$ <sup>1</sup> by Raman scattering.

In a second class of mixed-crystal systems, two-phonon frequencies are observed to occur at frequencies close to those of the end members. Here, the ratio of the strengths of the modes is approximately proportional to  $x$ . This is defined as "two-mode behavior." So far, two-mode behavior has been observed only in infrared spectra and primarily in covalent materials.<sup>18</sup> The only alkali halide in which two-mode behavior has been observed is  $\text{K}_{1-x}\text{Rb}_x\text{I}$ , which has been studied by Fertet and Perry<sup>20</sup> using infrared measurements.

The several models proposed to describe mixed-crystal behavior have been discussed by Chang and Mitra.<sup>18</sup> The virtual-crystal model<sup>17</sup> is one in which all masses and force constants are taken as averages weighted by the mixed-crystal composition. This model is at best qualitative and predicts a linear variation of frequencies with composition, but does not predict the features of the mixed system. The cluster model of Verleur and Barker,<sup>21</sup> based on short-range clustering, seems attractive, particularly in systems where clustering due to segregation arising from a miscibility gap is present. However, the model does not describe one-mode behavior in most cases. Further, even if it were assumed that the model is to be used only in systems where clustering is observed, it has to be modified considerably to take into account finite size and shape effects on the phonon frequencies of the clusters.

Other models which seek to describe mixed-crystal behavior by assuming nearest-neighbor interactions and random substitution are the linear-chain model of Matossi,<sup>22</sup> its extended form due to Langer, Park, and Euwema,<sup>23</sup> the random-element-isodisplacement (REI) models of Chen, Shockley, and Pearson,<sup>24</sup> and its modification, the MREI model of Chang and Mitra.<sup>18</sup> These describe only the  $q = 0$  phonons. They predict the frequency variation with composition and also attempt to derive conditions for one- or two-mode behavior, based on the masses of the ions involved. The Chang-Mitra criteria for the behavior of the  $q = 0$  phonons of mixed crystals have been found to hold in all systems examined so far.

In spite of the success of the above models, it is clear that a complete and correct theory of mixed crystals should involve the solution of the actual dynamical matrix of the mixed crystal, using a large enough unit so that the distribution of the ions in the mixed crystal is truly represented. In the case of a random mixed crystal, this would have to be a statistical average at best, so that the problem can be restricted to dimensions small enough to enable a solution to be effected.

The Green's-function approach has been used by several authors in an attempt to solve the mixed-crystal dynamics. The basis of most of these methods has been an iterative technique in which one sums an infinite series of Feynman-type diagrams. In a random crystal, containing many phonon branches, it is impossible to evaluate the diagrams. In the simplest of problems handled by these techniques, it has only been possible to obtain low-concentration approximations which give only a qualitative picture. Self-consistent approaches have been formulated by Taylor<sup>25</sup> and by Davies and Langer,<sup>26</sup> but the application to problems more complicated than that of a simple mass defect to systems higher than binary systems seems exceedingly complex. Pershan and Lacina<sup>27</sup> used a differential method based on the derivative of the mixed-crystal Green's functions  $G(c)$  [which assumes that  $G(c)$  is differentiable] and were able to describe the Raman and infrared data for  $(\text{Ca}, \text{Ba})_{1-x}\text{Sr}_x\text{F}_2$ <sup>19</sup> extremely well.

## III. EXPERIMENTAL TECHNIQUES

### A. Crystal Growth, Sample Preparation, and Analysis

The mixed-crystal samples were grown by the Kyropoulos method from pure alkali halides obtained from Merck. Pure-crystal seeds were used to grow KCl-KBr and KCl-RbCl from a melt consisting of a mixture of the pure halides in the desired proportion. For KBr-KI it was impossible to seed the melt with a pure-crystal seed because of the variation in the melting points.<sup>13</sup> Because of the miscibility gap below 200 °C, the KBr-KI

boules grown cracked in cooling. The best results, i. e., boules consisting of single-crystal regions, were obtained by using mixed-crystal seeds with  $x = 0.8$  for growing crystals with  $x > 0.6$ , and seeds with  $x = 0.1$  to  $0.2$  for those with  $x < 0.6$ . The systems  $\text{KCl}_{1-x}\text{I}_x$  has a miscibility gap even at high temperatures. Because of this, only one crystal with  $x = 0.04$  could be grown.

Because of the different melting points of the constituents the composition of the final boule is expected to be different from that of the melt. The compositions of the final samples used in the Raman and x-ray studies were determined by chemical methods and lattice-parameter measurements in the case of  $\text{KBr-KI}$  and  $\text{KCl-KI}$ , and by x-ray fluorescence analysis for  $\text{KCl-RbCl}$ .

Single-crystal pieces cleaved from the boules were used in the Raman experiments. The samples for x-ray-powder line-broadening studies were prepared by powdering the crystal and passing the powder through a  $44\text{-}\mu$ -size standard sieve. The powder was then pressed into a pellet 1 in. in diameter and 0.15–0.2 in. in thickness. The same powder was used in capillaries for the Debye-Scherrer photograph measurements for the lattice-parameter determination.

#### B. X-Ray Experiments

The lattice parameters were determined by the conventional Debye-Scherrer technique, using Cohen's method<sup>28</sup> to obtain the best value of the lattice parameter in each case.

The line-broadening studies were done on a GE x-ray diffractometer using filtered  $\text{Cu } K\alpha$  radiation as the source. A preliminary scan was made to obtain the positions of the lines. After the lines were indexed, the lines chosen for the line-broaden-

ing studies, viz., the (200) and (400) reflections, were scanned at a slow rate of 0.1 deg/min. This procedure was repeated on the pure and mixed crystals taking care to run the peaks out to the true background level. Where this was not possible, owing to the overlap of two peaks close in angular position, the extrapolation was made using the symmetry of the peaks and assigning suitable fractions of the observed intensity to the two peaks. The widths at half-maximum were then measured and the line broadening calculated.

#### C. Raman Experiments

The Raman-scattering experiments were done using conventional apparatus consisting of a Coherent Radiation model 52A argon-ion laser and a Spex model No. 1400 double monochromator with photon-counting electronics. The spectra were recorded using extremely slow scans for the spectra of low intensity.

A conventional optical Dewar was used in the optical studies. For the high-temperature studies of  $\text{KBr-KI}$ , a Pyrex cell with optical windows containing a central rod attached to a copper sample holder heated by nichrome winding was used.

The geometry and crystal orientation required to observe Raman spectra due to phonons or phonon combinations of  $A_{1g}$ ,  $E_g$ , and  $T_{2g}$  symmetry selectively have been described by Krauzman.<sup>29</sup> These orientations were used in the present work.

### IV. EXPERIMENTAL RESULTS AND DISCUSSION

#### A. X-Ray Results

##### 1. Lattice-Parameter Variation

The lattice-parameter variation of  $\text{KBr-KI}$  with composition is shown in Fig. 1. The average com-

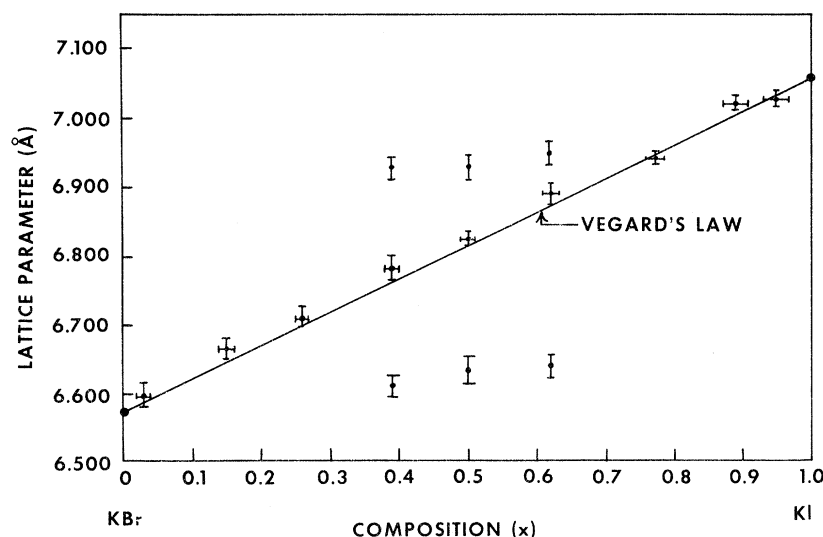


FIG. 1. Lattice-parameter variation of  $\text{KBr}_{1-x}\text{I}_x$  with composition  $x$ .

position indicated was determined by chemical methods, specially chosen to allow estimation of the iodide ion in the presence of the bromide ion.<sup>30</sup> The lattice parameters were determined from Debye-Scherrer photographs. The straight line is Vegard's law joining the lattice parameters of KI and KBr for which the values obtained are 7.055 and 6.575 Å, respectively (the NBS values are 7.040 and 6.585 Å). The error in the measured values of chemical composition is high for samples close to KI ( $\pm 4$  as against  $\pm 2\%$ ). This is because titration end points in the chemical method could not be determined accurately in this region owing to chemical interference. Each value is an average of five measurements done on samples taken from the Raman samples.

It is observed that for the extreme concentration ranges  $x < 0.3$  and  $x > 0.7$ , the system is characterized by a single fcc lattice parameter, while in the intermediate region three fcc phases, characterized by three lattice parameters, are observed. Because all the Debye-Scherrer lines could be indexed as those due to three fcc phases, the possibility of lowering of the "over-all symmetry" due to ordering can be ruled out. In each case, these three phases are the phase corresponding to the average concentration quenched in from above the critical temperature where the system is one phase, and the two phases corresponding to the concentration  $x \sim 0.08$  and  $x \approx 0.75$ , which are close to the miscibility limits of a moist sample as determined by Luova and Tannila.<sup>12</sup>

It was also observed that the lattice parameter of the single phase at the KBr-rich end has a larger deviation associated with it because the x-ray-powder lines in this case appeared rather broad. This point is discussed in Sec. IV A 2. Though the miscibility limit at the low- $x$  end is 0.08, as indicated by the sample with  $x > 0.3$ , samples with  $x = 0.15$  and 0.26 are apparently single phase. This is because these compositions probably contain an amount of the second segregated phase less than 7% of the total, and hence are below the limits of detection. In a completely segregated phase the "lever rule"<sup>28</sup> would indicate that the sample with  $x = 0.26$  should contain a fraction  $(0.26 - 0.08) / (0.75 - 0.08) = 25\%$  of the  $x = 0.75$  boundary phases. This is probably an indication that the sample had not segregated completely in the time ( $\sim 1$  yr) since its preparation. The lines for all low- $x$  crystals were broad, and the powder photograph for the  $x = 0.03$  sample contained a few of the most intense lines of pure KBr, indicating the presence of a small amount of KBr.

Thus the  $\text{KBr}_{1-x}\text{I}_x$  results clearly indicated the Vegard's-law variation in the single-phase region and the existence of three phases in the samples of intermediate concentration.

KCl-RbCl has been examined in detail before<sup>31</sup> and the existence of a continuous solid solution as indicated by the closeness of lattice parameters ( $\delta = 4.1\%$ ) verified. This was assumed in the present work.

## 2. Line-Broadening Studies

Our earlier small-angle x-ray-scattering studies of KCl-KBr<sup>1</sup> revealed no clusters smaller than an average linear dimension of  $\sim 200$  Å. Of the systems studied in the present work, powder lines of KBr-KI were considerably broadened and line-broadening studies were done on this system to look for clusters of a large size.

The conventional method<sup>32,33</sup> of determining the line broadening  $\Delta$  of the mixed-crystal line using its experimentally measured linewidth  $\Delta_1$  and the linewidth  $\Delta_0$  for the corresponding pure-crystal reflection is to use the equation

$$\Delta^2 = \Delta_1^2 - \Delta_0^2 .$$

Taylor<sup>34</sup> found that for ionic crystals this gave a larger estimate of the width and hence a smaller estimate of the cluster size, whereas a simple difference formula  $\Delta^1 = \Delta_1 - \Delta_0$  gave a lower value for the broadening and a larger estimate of the cluster size. Based on this, Taylor suggested that  $\Delta_c$ , the geometric mean of  $\Delta_0$  and  $\Delta_1$ , be taken as the corrected breadth. This technique has been observed to give a better estimate of cluster size by Cohen,<sup>35</sup> by comparison with independent electron-microscope measurements. This formula was used in the present work. After the broadening due to the mixed crystal is determined, the crystallite sizes responsible for the broadening are determined using the Scherrer equation.<sup>32</sup>

The reflections used were the (200) and (400) and the (111) and (222). Higher orders of the same reflections were used so that the cold-work broadening could be separated from the cluster-size broadening.<sup>35</sup> The (600) and (333) could not be used, because these overlap with the (442) and (511), respectively, and hence will not yield the correct widths. In all cases except one, the crystallite sizes obtained from the higher-order reflections were within 20% of that from the lower one. This indicated that cold-work broadening was not significant. As only an approximate estimate of the cluster size was desired, the Warren technique<sup>36</sup> for separating the cold-work broadening was not used.

The KCl-KBr crystals used in our earlier study<sup>1</sup> were examined by this technique. The difference between mixed-crystal and pure-crystal linewidths was small. Estimated crystallite sizes ranged from 4000 to 6000 Å (to within 20%). This range of crystallite size is in the limit of validity of the method used. Thus, because it is not possible to

TABLE II. Line-broadening analysis of  $\text{KBr}_{1-x}\text{I}_x$ .

Av. chemical composition	Phases present (x ray)	Av. particle size of phase ( $\text{\AA}$ )	Approx. percentage <sup>a</sup> (from peak areas)
0.15	0.12	600	100
0.26	0.25	300	100
0.39	(i) 0.72	580	20
	(ii) 0.4	1650	50
	(iii) 0.08	500	30
0.50	(i) 0.74	530	43
	(ii) 0.50	1450	24
	(iii) 0.13	550	33
0.62	(i) 0.74	600	50
	(ii) 0.60	1500	35
	(iii) 0.09	450	15

<sup>a</sup>Percentage composition approximate because corrections due to the polarization factor and atomic scattering factor have been neglected.

push the accuracy of the method beyond this range, we estimate a lower limit to grain size in the  $\text{KCl-KBr}$  system as 4000  $\text{\AA}$ .

The results on the  $\text{KBr-KI}$  system are enumerated below.

(i) The linewidths for the high- $x$  (near  $\text{KI}$ ) samples were close to the pure-crystal values, showing only the shift due to average lattice-parameter variation, so that the crystallite size may be assumed to be essentially "infinite" ( $\gtrsim 4000 \text{\AA}$ ).

(ii) The crystals with low values of  $x$ , i. e.,  $x < 0.25$ , gave lines corresponding to single-phase systems but the lines were broadened considerably. The estimates of grain sizes and percentage compositions are given in Table II.

(iii) The three-phase region contained the two boundary phases close to those found by Luova and Tannila<sup>12</sup> for a moist sample, and the quenched-in high-temperature phase. Table II summarizes the results.

The sample with  $x = 0.26$  indicated in Table II had been grown approximately two months before the measurements were made. Samples with  $x = 0.40$  grown a year before showed widths 30–40% higher for higher-order reflections, indicating that cold work is higher in these. In all the other samples, crystallite sizes differed only by 8–10% when calculated from (200) and (400) reflections.

Thus it is clear that the crystals of  $\text{KBr-KI}$  in the intermediate composition range segregated with crystallites of the different phases with cluster sizes  $\sim 300\text{--}500 \text{\AA}$  of the minor component. The mixed crystals close to the  $\text{KBr}$  end of the composition also showed small grain size, indicating the presence of segregated phases in amounts below limits of detection ( $\leq 7\%$ ).

### 3. Other Attempts to Obtain Segregated Phase in $\text{KBr}_{1-x}\text{I}_x$

In principle, light (Mie) scattering, optical-microscope, and scanning-electron-microscope

studies can be used to estimate the particle sizes. The microscopic methods are particularly attractive, because under favorable conditions they can yield an actual picture of the distribution of the regions of different phases. All attempts using these techniques failed, basically because the phases to be differentiated were too close in physical properties.

### B. Raman Spectra

The second-order spectra of the pure alkali halides have been studied by Krauzman<sup>37</sup> and our results for the pure end members are in agreement with his. In all the systems studied by us a relatively high-impurity concentration, of the order of 3%, had to be reached before observable impurity-induced first-order scattering was obtained. Even at these concentrations, the induced first-order spectra were only of the same intensity as the second-order spectra. Hence, the temperature dependence of the spectra had to be studied to distinguish between first- and second-order spectra. Our most extensive studies were done primarily at room temperature.

The discussion of the Raman spectra is best done by examining the results for each system separately and then describing the features common to all the systems and those that differ.

Our earlier results for the  $\text{KCl-KBr}$  system are worth reviewing briefly to enable easy comparison with the systems studied in the present work. The induced first-order spectra for  $\text{KCl-KBr}$  were of  $A_{1g}$  and  $T_{2g}$  symmetry. At either end of the composition range, the  $A_{1g}$  features closely resembled the one-phonon density of states of the pure crystals as calculated by Page.<sup>38</sup> A low-frequency mode at approximately  $118 \text{ cm}^{-1}$  was observed at low concentrations of  $\text{KCl}$ , decreasing in intensity as the bromine content increased and disappearing by  $x = 0.3$  (30 at. %  $\text{KBr}$  in  $\text{KCl}$ ). It was suggested by us in the earlier paper<sup>1</sup> that this might be a resonant mode of  $\text{Br}$  in  $\text{KCl}$ . In view of the appearance of an identical band in  $\text{KCl}_{1-x}\text{I}_x$ , and by comparison with the results on  $\text{KBr}_{1-x}\text{I}_x$ , this band can instead be identified as the  $\text{LA}(X)$  phonon of pure  $\text{KCl}$ . A careful study of the spectra also reveals first-order bands corresponding to the  $\text{LO}(\Gamma)$  of  $\text{KCl}$  at the lowest concentration and the  $\text{LA}(X)$  and  $\text{LO}(\Gamma)$  phonons of  $\text{KBr}$  at the  $\text{KBr}$  end of the concentration range. In this connection we note that the  $\text{LO}(\Gamma)$  is forbidden by selection rules in a cubic site, but allowed in a tetragonal symmetry. Thus the weak peak observed may be due to a lowering of local symmetry.

As  $x$  increased, in  $\text{KCl}_{1-x}\text{Br}_x$ , a single first-order peak of  $A_{1g}$  symmetry was the most salient feature of the mixed-crystal spectra, the frequency of the peak shifting linearly with composition. When a

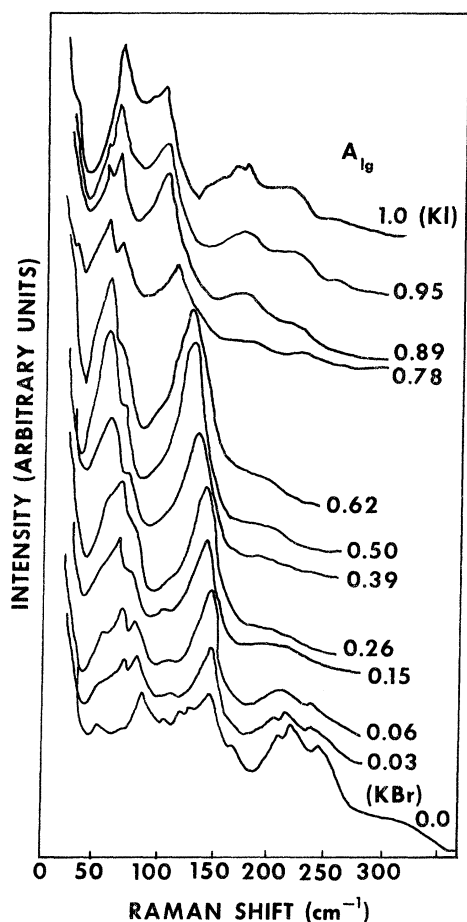


FIG. 2.  $A_{1g}$  spectra of  $KBr_{1-x}I_x$  as a function of composition  $x$  at 300 K.

frequency-versus-composition graph was plotted, the straight-line fit intersected the pure-crystal axes at values close to those of the  $TO(X)$  phonons of KCl and KBr. A possible reason for the  $TO(X)$  phonon being the major contributor to the Raman scattering is the fact that the phonon density of states is highest near the  $TO(X)$  frequency for both KCl and KBr,<sup>39,40</sup> and hence may be expected to be so for the mixed crystal as well. A weak  $T_{2g}$  peak was also observed. However, this varied very little in frequency and did not correspond to any easily identified phonon. No first-order spectrum of  $E_g$  symmetry was observed.

#### 1. $KCl_{1-x}I_x$

Only one composition,  $x = 0.04$  of this system, was examined. The Raman spectrum of  $A_{1g}$  symmetry observed had a single first-order peak and looked identical to the  $KCl_{1-x}Br_x$  for  $x = 0.03$ . No first-order scattering due to phonons of  $E_g$  or  $T_{2g}$  symmetry was observed.

The single low-frequency peak observed at the

same frequency in KCl:Br and KCl:I indicates that it is a mode of the pure crystal KCl, activated in Raman scattering by the impurity, rather than a resonant mode due to a particular impurity.

#### 2. $KBr_{1-x}I_x$

At first glance, this system is expected to be completely analogous to the KCl-KBr system. However, the miscibility gap in this system presents certain problems and a direct comparison of the results can be made only after accounting for the finite crystal effects arising from the small sizes of the clusters.

No infrared work on this system has been reported. Kan<sup>41</sup> studied the ultraviolet absorption and luminescence properties for samples with various values of  $x$ . No unexpected effects were observed, even though his x-ray studies indicated that the crystals of intermediate composition consisted of segregated phases.

*a.  $A_{1g}$  spectra.* In this system, too, the most striking features are of  $A_{1g}$  symmetry. No first-order feature of  $E_g$  symmetry is found. The variation of the  $A_{1g}$  Raman spectra with composition is shown in Fig. 2. The first and last spectra correspond to the pure crystals. The lowest concentration examined was  $x = 0.01$ , and for this no noticeable difference was found in the spectrum from that of pure KBr. The spectra, however, do not vary continuously with concentration as in the case of KCl-KBr and the results of different concentration ranges are best discussed separately.

*b. Range  $1:0 < x < 0.10$ .* The lowest concentration for which first-order effects were observed was  $x = 0.03$ . The Raman spectra of the  $x = 0.03$  sample (Fig. 3) show three first-order peaks, one at  $\sim 71 \text{ cm}^{-1}$ , a very weak one at  $118 \text{ cm}^{-1}$ , and a strong band at  $148 \text{ cm}^{-1}$ . The second-order part of the spectrum still closely resembles that of pure KBr in shape, but is shifted towards lower frequencies, the cutoff being  $\sim 15 \text{ cm}^{-1}$  below that of KBr. The 71- and  $148\text{-cm}^{-1}$  peaks grow in intensity where the concentration changes to  $x = 0.06$ , but the  $118\text{-cm}^{-1}$  peak still remains weak. In both the spectra ( $x = 0.03$  and  $0.06$ ), the  $71\text{-cm}^{-1}$  band overlaps with what is resolved from the  $2TA(X)$  second-order band.

*c. Range  $2:0.15 \leq x \leq 0.62$ .* In this range, the spectra are markedly different from those of either of the end regions. For  $x = 0.15$ , the spectrum still resembles the  $x = 0.06$  spectrum in the main first-order band at approximately  $150 \text{ cm}^{-1}$ , but the high-frequency second-order region is markedly different. The  $71\text{-cm}^{-1}$  region no longer consists of two resolved peaks but of a broad intense band. Its temperature dependence indicated that this band is primarily due to second-order scattering even though at 300 K its intensity is greater than

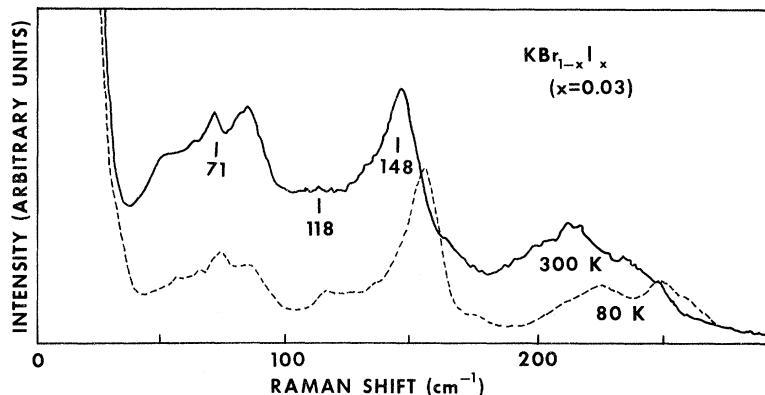


FIG. 3. Temperature dependence of  $A_{1g}$  spectrum of  $\text{KBr}_{0.97}\text{I}_{0.03}$  ( $x=0.03$ ).

the first-order band.

For  $x=0.26$ , the spectrum essentially consists of two intense bands. The lower-frequency band extends from 50 to 100  $\text{cm}^{-1}$ , peaks at 75  $\text{cm}^{-1}$ , and has a shoulder at about 80  $\text{cm}^{-1}$ , and corresponds apparently to the mixed-crystal  $2\text{TA}(X)$  combination band, judging from its evolution from the  $2\text{TA}(X)$  peak of the pure-KBr spectrum. This band is as intense as the first order at 300 K but has a temperature dependence indicative of second-order scattering. The higher-frequency band has a peak at  $\sim 142 \text{ cm}^{-1}$  and is of first order. There is very little second-order scattering in the frequency region higher than about 150  $\text{cm}^{-1}$  (Fig. 2).

The general structure described above, a broad low-frequency second-order band and a first-order band at a higher frequency, persists throughout the range  $0.26 \leq x \leq 0.62$ . Both of the peaks move towards lower frequencies but very slowly as concentration is changed. The intensity of the peaks is approximately constant with composition and is higher than the intensities at either end. The Rayleigh peaks in this region were broader than those in the end regions, probably owing to the scattering by the clusters of different phases indicated by the x-ray experiments.

*d. Range  $3:1 > x \geq 0.78$ .* All efforts to grow crystals with a composition of approximately 0.7 resulted in crystals with  $x > 0.75$  or  $x < 0.65$ . The spectrum of the crystal with  $x = 0.78$  was markedly different from that of the  $x = 0.62$  crystal. This range of concentration is probably best examined from the higher end, starting with the spectrum for KI ( $x = 1.0$ ), which, of course, is a purely second-order spectrum. When 5-at. % KBr is added ( $x = 0.95$ ), two first-order peaks are observed. The first peak is a weak band at  $\sim 48 \text{ cm}^{-1}$ . It overlaps with but is resolved from the strong second-order peak, which is primarily due to the combinations  $2\text{TA}(X)$ ,  $\text{TO} - \text{TA}(X)$ ,  $\text{TO} - \text{TA}(\Delta)$ , and  $2\text{TA}(\Sigma)$ . The second first-order band is at  $\sim 110 \text{ cm}^{-1}$  and cannot be resolved from the second-order peak due

primarily to  $2\text{LA}(X)$ . On cooling, however, it is observed that this first-order band is very narrow and the frequency value at 80 K is 108  $\text{cm}^{-1}$ . This temperature dependence is very striking and is shown in Fig. 4. The low-temperature data (80 and 20 K) also indicate another weak first-order band at 90  $\text{cm}^{-1}$ . This persists in the  $x = 0.95$  and  $x = 0.78$  samples. As in the case of  $\text{KCl}_{1-x}\text{Br}_x$ , the spectrum closely resembles the density of states of the unperturbed  $A_{1g}$  phonons of pure KI at the heavy end of the concentration. As the bromine concentration increases, i. e., for  $x = 0.95$  and 0.89, the 51- $\text{cm}^{-1}$  peak shifts slightly to higher frequencies and gains in intensity, while the second-order peak is relatively weak. The higher-frequency band appears to go down in intensity, but low-temperature results indicate that this apparent loss is because the second-order scattering is weak, and also due to the broadening of the line. It is also observed that though the first-order spectrum for  $x = 0.78$  looks very similar to those for  $x > 0.78$ , the high-frequency region of the second-order background resembles that of the intermediate  $x$  region discussed previously. The first-order frequencies at the extreme concentration values ( $x = 0.03$  and  $x = 0.95$ ) are close in magnitude to certain pure-crystal phonon frequencies and these are indicated in Table III. All frequency values

TABLE III. First-order bands of  $\text{KBr}_{1-x}\text{I}_x$  compared with pure-crystal phonon frequencies.

$x$	Observed phonon frequency	Comparable pure-crystal phonon frequencies		Phonon-type and symmetry
		KBr (400 K) ( $\text{cm}^{-1}$ )	KI (95 K) ( $\text{cm}^{-1}$ )	
0.03	71	72		LA(X)
0.06	118	115		TO(I)
	148	120		TO(X)
0.95	48		51	LA(X)
0.89	90 (80 K)		91	TO(L)
	$\sim 110 \text{ cm}^{-1}$		103	LO(X)
				103

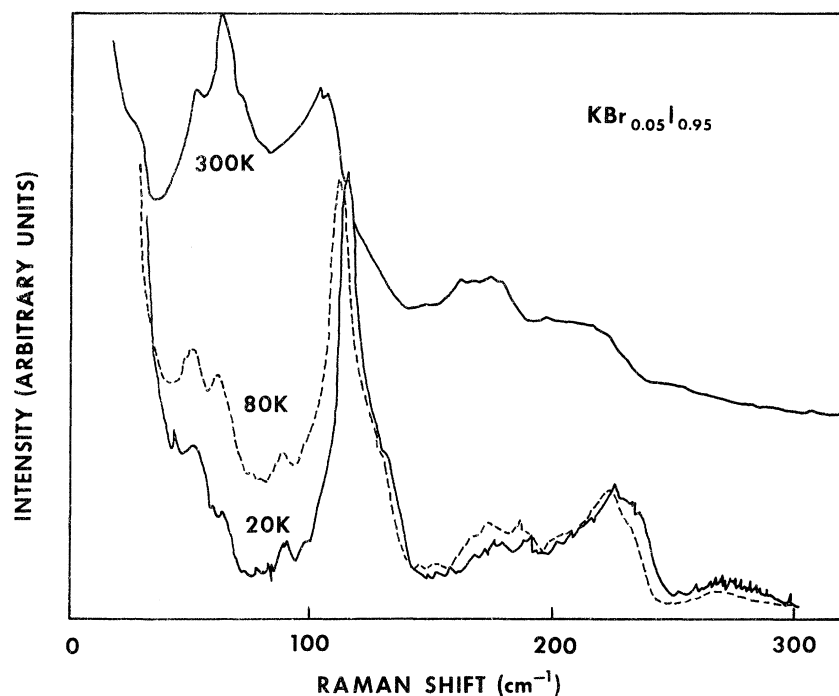


FIG. 4. Temperature dependence of  $A_{1g}$  spectrum of  $\text{KBr}_{0.05}\text{I}_{0.95}$  ( $x=0.95$ ).

are at 300 K except where indicated.

*e. Variation of  $A_{1g}$  frequency with concentration.* The variation of the first-order peak of  $A_{1g}$  symmetry with  $x$  is shown in Fig. 5. The three points near  $x=1$  (KI) lie in a straight line, which cuts the KI axis close to the  $\text{TO}(X)$  frequency of KI. A dramatic rise in frequency is seen in the next point, corresponding to the sudden change in the spectrum noted in Fig. 2. This break is observed to occur at a concentration close to the limit of miscibility at the KI end. No similar break is observed at the KBr end. This break can be shown to be due to finite crystal effects and the details have been published elsewhere.<sup>42</sup> The only point

of relevance here is that the frequencies can be "corrected" down to the infinite crystal values as shown in Fig. 5. When this is done, the graph extrapolates to the  $\text{TO}(X)$  frequency of KBr, as is to be expected from the results of KCl-KBr. Here we note again that the phonon density of states in KBr and KI are highest at the  $x$  point.<sup>40,43</sup>

*f.  $T_{2g}$  spectra.* These spectra (Fig. 6) also show distinct features in the middle range of concentration. The first-order features are very weak at either end and consist of a broad band at  $\sim 110 \text{ cm}^{-1}$  for the intermediate concentrations. Again, this band is three times as intense as the first-order region of the spectrum at either end of the con-

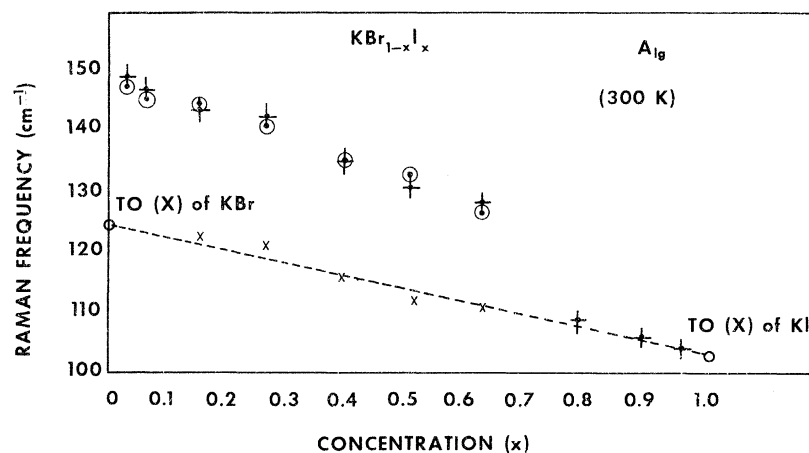


FIG. 5. Concentration dependence of the  $A_{1g}$  peak of  $\text{KBr}_{1-x}\text{I}_x$  at 300 K, corrected for finite crystal effects; crosses, experimental points;  $x$ 's, experimental values multiplied by the correction factor (the Fröhlich ratio). The dotted line joins the  $\text{TO}(X)$  frequencies of KBr and KI.

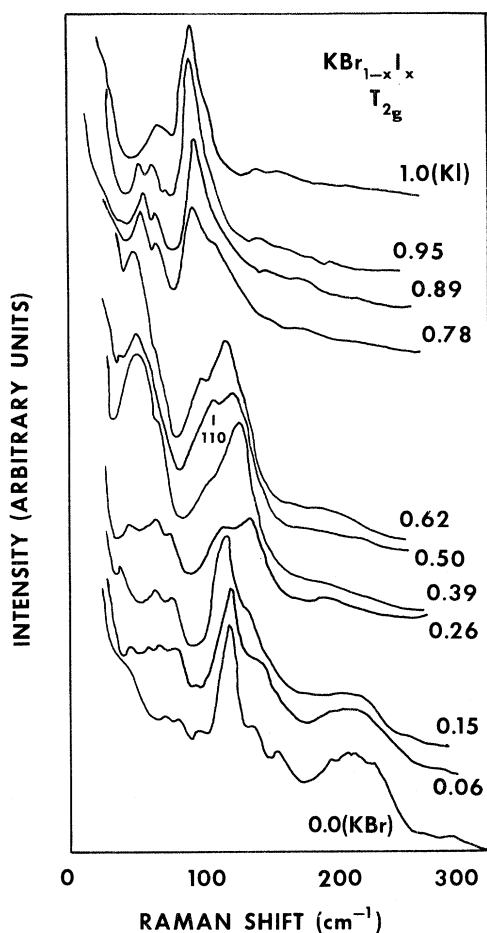


FIG. 6.  $T_{2g}$  spectra of  $\text{KBr}_{1-x}\text{I}_x$  as a function of composition  $x$  at 300 K.

centration range. The frequency-concentration graph, however, does not show as sharp a break at these concentrations as the  $A_{1g}$  frequency variation. The observed band is broad and the peak positions cannot be obtained.

Attempts were made to see whether any lowering of symmetry was observable in the mixed crystals. Usually, the  $x$ ,  $y$ , and  $z$  axes (cleavage directions) are treated as interchangeable in recording the polarized spectra. For three samples of intermediate concentration,  $x$ ,  $y$ , and  $z$  axes were defined, and their separate identities maintained while taking the spectra with all possible settings and polarizations. No distinction between the directions was observable, either in peak positions or average intensity of spectra, a result which indicates that, on the average, a "cubic" symmetry was still maintained.

*g. High-temperature spectra.* The peculiarities of the spectra of the mixed crystals in the intermediate concentration range can be attributed to the small sizes of the regions of different phases.

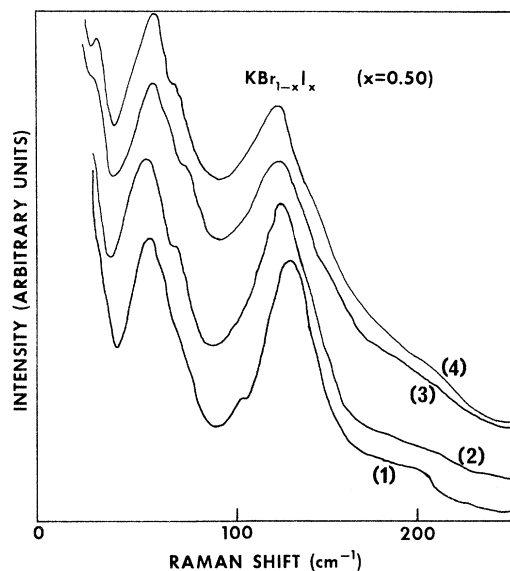


FIG. 7. High-temperature spectra of  $\text{KBr}_{1-x}\text{I}_x$ : (1) 293 K, (2) 353 K, (3) 453 K, (4) 493 K.

The high-temperature spectra of the crystals of intermediate concentrations were studied in the hope that the spectrum above the critical temperature ( $200^\circ\text{C}$ ) may show a marked change owing to the single-phase nature of the system above this temperature.

The temperature variation of the spectrum for  $x = 0.5$  is shown in Fig. 7. Only the anharmonic effects—frequency shift and line broadening—and the different temperature dependence of second-

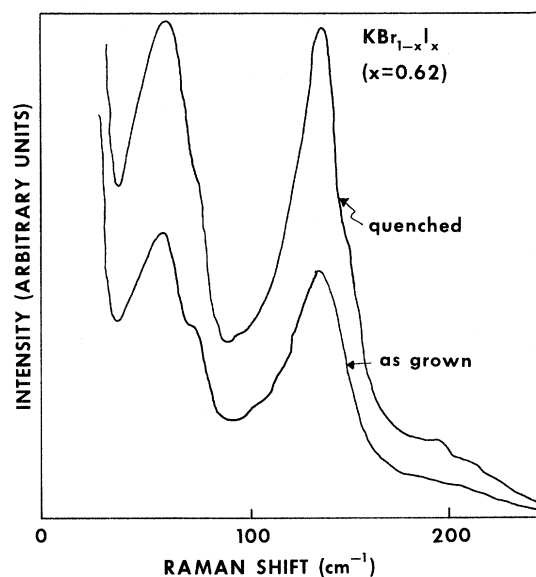


FIG. 8.  $A_{1g}$  spectra of quenched and as-grown samples of  $\text{KBr}_{1-x}\text{I}_x$  ( $x=0.62$ ) at 300 K.

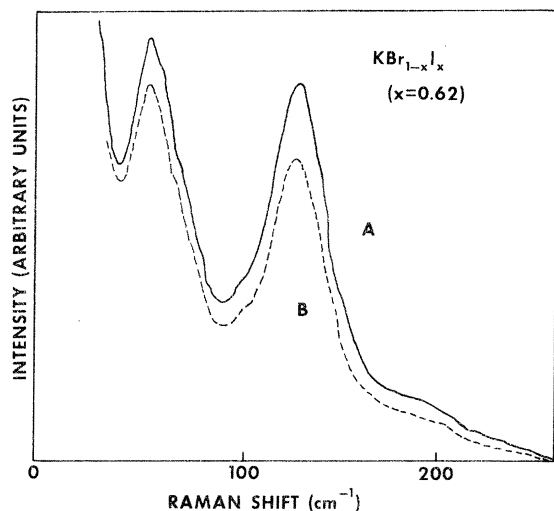


FIG. 9.  $A_{1g}$  spectra of (A) newly grown and (B) aged samples of  $\text{KBr}_{1-x}\text{I}_x$  ( $x=0.62$ ) at 300 K.

and first-order spectra were evident. The crystal was maintained at  $215^\circ\text{C}$  for 5 h. No noticeable change occurred in the spectrum. This is probably because the diffusion coefficients at this temperature are still too low for significant reordering of the structure to take place. When the crystal is cooled back to room temperature, the spectrum is identical to the original room-temperature spectrum.

Spectra of samples cooled slowly from  $50^\circ\text{C}$  below their melting point to room temperature were the same as the spectra for the original samples. A crystal ( $x=0.5$ ) was heated to  $50^\circ$  below the melting point, maintained at that temperature for 48 h, and quenched to room temperature in order to "freeze in" the high-temperature phase. Though the crystal cracked on quenching, samples of size large enough to record the Raman spectra could be obtained. The spectra of these samples were similar to the others, with one distinction—the second- and first-order peaks had their intensity concentrated in a narrower range of frequency at the center of the original room-temperature bands. This is shown in Fig. 8. This is indicative of the fact that this sample contained more of the intermediate high-temperature phase than the original samples. Figure 9 shows the spectra of a new (three days after growing) sample and its spectrum 15 months later, when the sample was visibly clouded, probably due to segregation. No significant change is observed.

Another interesting point, suggesting the application of Raman spectroscopy to the observation of ordering, can be noted here. Figure 10 shows the room-temperature spectra of two Raman samples differing in composition compared with their corresponding spectra at 80 K. It is observed that

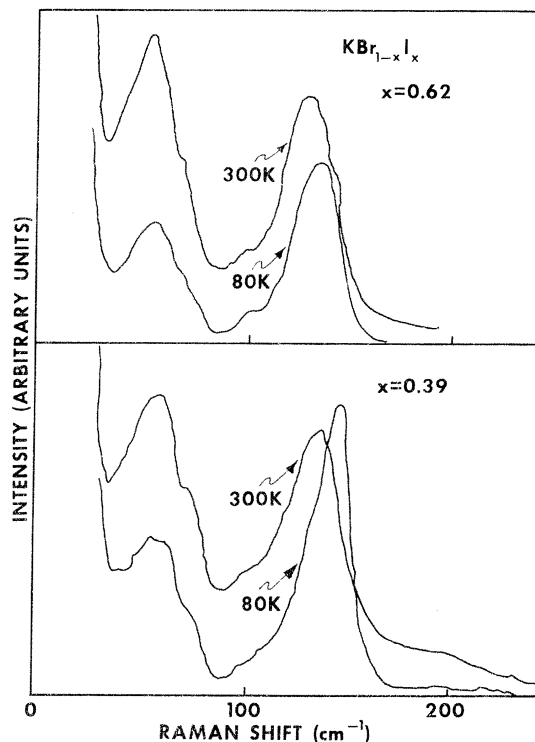


FIG. 10. Temperature dependence of  $A_{1g}$  spectra of samples of  $\text{KBr}_{1-x}\text{I}_x$  for  $x=0.62$  and  $x=0.39$  showing difference in line broadening with temperature.

in both cases the temperature ratio for one-phonon processes is obtained when the areas of the bands are taken. However, in the case of the sample with  $x=0.62$ , the width of the line at low temperature is close to the value at 300 K, while in the case of the sample with  $x=0.39$  the width at 80 K is con-

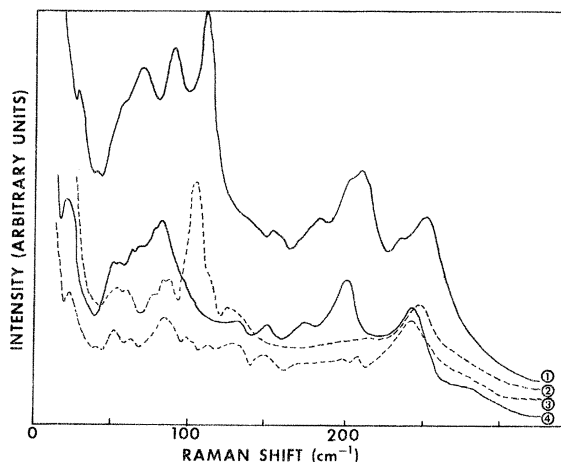


FIG. 11. Comparison of  $A_{1g} + 4E_g$  and  $E_g$  only spectra for  $\text{K}_{0.15}\text{Rb}_{0.85}\text{Cl}$  and pure  $\text{RbCl}$ : (1)  $A_{1g} + 4E_g$  for  $\text{K}_{0.15}\text{Rb}_{0.85}\text{Cl}$ , (2)  $E_g$  only for  $\text{K}_{0.15}\text{Rb}_{0.85}\text{Cl}$ , (3)  $E_g$  only for pure  $\text{RbCl}$ , (4)  $A_{1g} + 4E_g$  for pure  $\text{RbCl}$ .

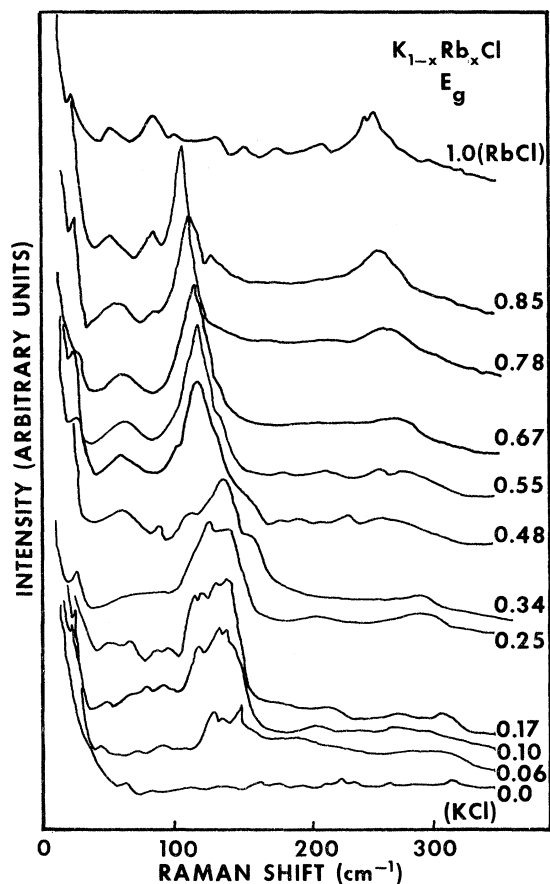


FIG. 12.  $E_g$  spectra of  $K_{1-x}Rb_xCl$  as a function of composition  $x$  at 300 K.

siderably less. The width of the bands observed here arises from anharmonic effects and from the local variation in symmetry. As anharmonic effects for the two crystals can be assumed to be approximately the same, the narrowing of the line

from the  $x = 0.39$  sample indicates that there is a much higher local order at this composition than in the other. The chance of local ordering is higher for the case where the "impurity ion" is larger and this is indeed seen to be the case.

### 3. $K_{1-x}Rb_xCl$

This system was not studied by x-ray techniques. However, in view of previous works<sup>31</sup> on the system and as the lattice-parameter deviation  $\delta$  for this system is less than that for KCl and KBr, it can be assumed to be a single-phase, random, substitutional mixed crystal. The composition of the samples was determined by x-ray fluorescence analysis.

The most striking feature of the Raman spectra for this case is that the induced first-order spectra are mainly of  $E_g$  symmetry with a weaker spectrum of  $T_{2g}$  symmetry. No  $A_{1g}$  scattering was observed. This is shown in Fig. 11, which shows the  $A_{1g} + 4E_g$  spectra for  $K_{0.1}Rb_{0.9}Cl$  and for pure RbCl and the  $E_g$  spectrum alone for the mixed crystal. Here, the induced peak is seen clearly to be of  $E_g$  symmetry.

Figure 12 shows the  $E_g$  spectra as a function of concentration. At the low- $x$  end, i. e., near KCl, the first-order features strongly resemble the  $E_g$  density of states of perturbed phonons calculated by Page for a positive-ion impurity with no force constant change and observed by Harley, Page, and Walker<sup>4</sup> in  $KCl:Ti^+$ . The induced spectra in the present case, however, are very much weaker than those in  $KCl:Ti^+$ . Another point worth noting is that even the lowest concentration of  $Rb^+$  here—5 mol%—is much larger than the concentration of  $Ti^+$  ( $\leq 1$  mol%) used by them. As  $x$  increases, the spectrum reduces to a single symmetric peak. Again for high  $x$  (near RbCl), the peak resembles the RbCl perturbed-phonon density of states also

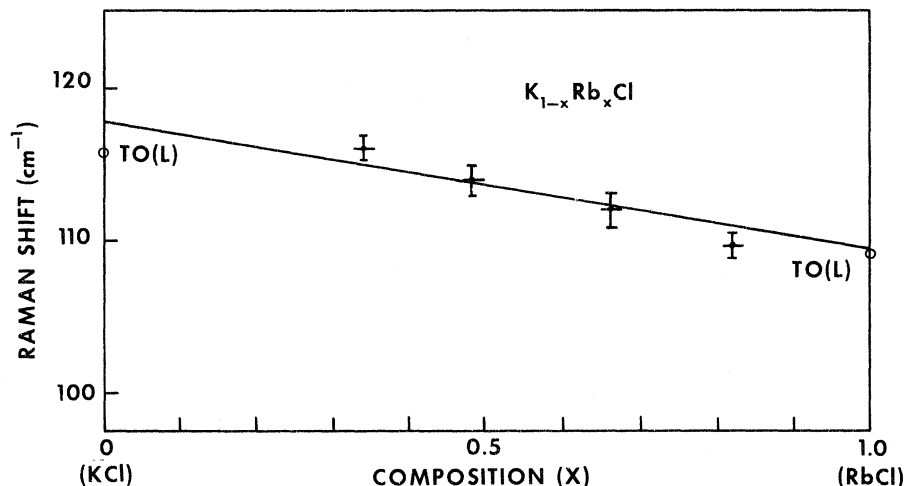


FIG. 13. Concentration dependence of  $E_g$  peak of  $K_{1-x}Rb_xCl$  with composition at 300 K.

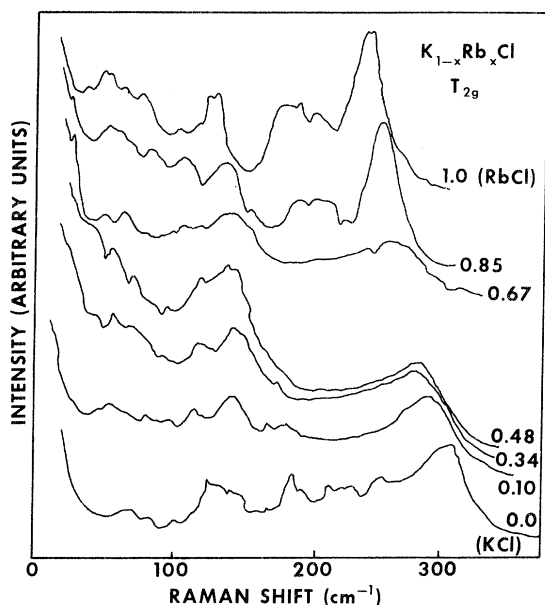


FIG. 14.  $T_{2g}$  spectra of  $K_{1-x}Rb_xCl$  as a function of composition  $x$  at 300 K.

calculated observed by Harley, Page, and Walker. The calculated density of states that most resembles the experimental peak is that for a fractional force constant change  $\delta k/k = +0.1$ .

The variation of frequency with concentration can be plotted (Fig. 13). The first-order peak position can be unambiguously obtained only for the intermediate compositions. These points can be fitted by a straight line and the extrapolation of the straight-line fit intersects the KCl and RbCl axes at 117 and 106  $\text{cm}^{-1}$ , respectively. These values are close to the  $TO(L)$  frequencies of KCl and RbCl, viz., 116  $\text{cm}^{-1}$  (115 K) and 109  $\text{cm}^{-1}$  (300 K), respectively. The room-temperature value of the KCl  $TO(L)$  phonon is probably  $\sim 110 \text{ cm}^{-1}$ , very close to that of RbCl. Though the  $L$  point is one of the critical points for the fcc structure, the phonon density of states at the  $TO(L)$  frequency for both KCl and RbCl is less than half the maximum value.<sup>39,44</sup>

$T_{2g}$  spectra. The intensity of the first-order  $T_{2g}$  spectrum (Fig. 14) is approximately 70% of that of the  $E_g$  spectrum, and the spectral features again resemble the calculated density of states for extreme values of  $x$ . The extremely broad features, however, make the determination of any peak position impossible.

Although the mixed system KBr-RbBr has been investigated for a range of compositions by neutron scattering,<sup>16</sup> and KI-RbI has been studied in detail by Fertel and Perry<sup>20</sup> using Kramers-Kronig analysis of infrared reflectivity spectra, the only optical work on KCl-RbCl is the unpublished infrared

transmission measurements of Mitsubishi.<sup>45</sup> The frequency of the  $TO(\Gamma)$  in this case was found to vary linearly with concentration. However, the samples were thin films and no determination of the composition was made after their evaporation. In the KBr-RbBr system, the variation of frequency with composition was observed to be small.

## V. GENERAL TRENDS IN MIXED-CRYSTAL SPECTRA

### A. Symmetry of Induced First-Order Spectra

Of the three systems studied in detail in the present work,  $KCl_{1-x}Br_x$  and  $KBr_{1-x}I_x$  involve negative-ion substitution, while  $K_{1-x}Rb_xCl$  involves positive-ion substitution. One striking distinction between negative- and positive-ion-induced first-order spectra is that in the former case the spectra are due to phonons of  $A_{1g}$  and  $T_{2g}$  symmetry while in the latter case the spectra are due to phonons of  $E_g$  and  $T_{2g}$  symmetry. An examination of other experiments on impurity-induced Raman scattering indicates that the rule is general in its application to impurities in ionic crystals. Including the systems in the present study, the impurity systems of alkali halides involving positive-ion substitution that have been studied so far are  $Tl^+$  ion in KCl, KBr, KI, and RbCl,  $NaCl: Ag^+$ ,<sup>46</sup> and  $KCl: Rb^+$  and  $RbCl: K^+$ . In all these, only spectra of  $E_g$  symmetry and weaker  $T_{2g}$  spectra were observed. The negative-ion-substituted systems studied are  $KCl: Br^-$ ,  $KCl: I^-$ ,  $KBr: Cl^-$ , and  $KBr: I^-$  in the present work and  $BaF_2: H^-$ .<sup>47</sup> In all these, the dominant induced spectra were of  $A_{1g}$  and  $T_{2g}$  symmetry and no significant contribution from  $E_g$  phonons could be observed.

### B. Pure-Crystal Density of States and Phonons

In all the systems studied, the low-concentration spectra clearly reflect the predominant features of the pure crystal density of states. This is to be expected from theory for low impurity concentrations, as the predominant frequency-dependent term in the cross section is the phonon density of states. However, it is surprising that the pure-crystal features should be predominant even at impurity concentrations as high as 10 at. %, where the impurity has long ceased to be of merely a perturbation in the host crystal. This fact can be used, however, to obtain the temperature dependence and other characteristics of certain phonons of crystals which do not exhibit first-order Raman scattering in the pure state.<sup>48</sup>

### C. Mixed-Crystal Phonons

It is evident from the spectra of crystals in the intermediate concentration range that the scattering is from mixed crystals. Though, as discussed in Sec. II, periodicity and the definition of the Brillouin zone cannot be rigorously justified in a

mixed crystal, it appears that a Brillouin-zone classification of the phonons is still useful to a certain extent. For instance, in  $\text{KCl}_{1-x}\text{Br}_x$  and  $\text{KBr}_{1-x}\text{I}_x$ , the  $\text{TO}(X)$  phonons of the mixed crystals appear to give the contribution to Raman scattering.

In pure KBr, KI, and KCl, the density-of-states peak is close to the  $\text{TO}(X)$  frequency, though not exactly at  $X$  as pointed out by Copley *et al.*<sup>39</sup> Thus it is reasonable to expect that the density of states in the corresponding mixed systems, too, is higher at the  $X$  point. This may be why the  $\text{TO}(X)$  frequency appears most strongly in the Raman spectra of  $\text{KBr}_{1-x}\text{I}_x$  and  $\text{KCl}_{1-x}\text{Br}_x$ . However, this cannot explain why the extrapolation of KCl-RbCl indicates an intersection at a value different from any of the major critical points. Thus the predominant phonon of the mixed crystal as observed in the Raman spectra cannot be explained on the basis of the density-of-states term in the cross section alone.

The fact that all peaks are broad,  $\geq 20 \text{ cm}^{-1}$ , is probably a reflection of the variation of the local composition. It is this variation that makes a definite symmetry analysis impossible.

#### VI. SUMMARY AND CONCLUSIONS

Certain general features of mixed alkali halides as evidenced in their Raman spectra have been obtained in the present experimental study. Zone-boundary phonons seem to be the main contributors

to Raman scattering in the mixed crystals. This may be a mere reflection of the fact that these also happen to correspond to the peaks in the density of states. A number of bands, at frequencies corresponding to phonons of the pure crystal at high-symmetry points, are observed even at high concentration of impurities.

This study also indicates that in spite of uncertainties in assignments, Raman-scattering experiments are capable of revealing general systematics of at least some of the phonons of the mixed crystals. Neutron experiments can aid in the understanding of the data to some extent, but uncertainties like those in symmetry assignments due to the inherent random variation in local symmetry cannot be removed. In the present work, all information of general characteristics has been derived using Raman scattering, and it seems that Raman experiments on many more ionic crystals with substitutional impurities would give an insight into the mechanism and the relation between the value of the impurities and the electron-phonon coupling.

Experiments on other mixed systems, e. g.,  $\text{K}_{1-x}\text{Rb}_x\text{I}$ , known to be a two-mode system, or on systems with miscibility gaps should also prove interesting. X-ray studies of the detailed distribution of ions in some of the impurity systems may also give a clue to the mixed-crystal phonon behavior.

<sup>†</sup>Work supported by the Advanced Research Projects Agency through the Northwestern University Materials Research Center and by the Army Research Office, Durham.

\*Present address: Materials Science Department, Northwestern University, Evanston, Ill. 60201.

‡Present address: Department of Physics, Arizona State University, Tempe, Ariz. 85281.

<sup>1</sup>I. Nair and C. T. Walker, *Phys. Rev. B* **3**, 3446 (1971).

<sup>2</sup>R. Loudon, *Adv. Phys.* **13**, 423 (1964).

<sup>3</sup>A. A. Maradudin, *Solid State Phys.* **19**, 1 (1967).

<sup>4</sup>R. T. Harley, J. B. Page, and C. T. Walker, *Phys. Rev. B* **3**, 1365 (1971).

<sup>5</sup>J. P. Hurrell, S. P. S. Porto, T. C. Damen, and S. Mascarenhas, *Phys. Lett.* **25A**, 194 (1968).

<sup>6</sup>F. A. Matsen and J. Y. Beach, *J. Am. Chem. Soc.* **63**, 3470 (1941).

<sup>7</sup>A. V. Tobolsky, *J. Chem. Phys.* **10**, 187 (1942).

<sup>8</sup>M. Ahte, *Ann. Acad. Sci. Fenn. A6*, No. 313 (1969).

<sup>9</sup>J. A. Wasastjerna, *Soc. Sci. Fennicae, Commentationes Phys. Math.* **15**, No. 3 (1949).

<sup>10</sup>P. Luova, *Ann. Acad. Sci. Fenn. A6*, **155** (1964).

<sup>11</sup>G. S. Durham and J. A. Hawkins, *J. Chem. Phys.* **19**, 149 (1951).

<sup>12</sup>P. Luova and O. Tannila, *Suomen Kemistilehti* **B39**, 220 (1966).

<sup>13</sup>P. Luova and M. Muurinen, *Ann. Univ. Turkuensis AI.*, No. 110 (1967).

<sup>14</sup>J. Retgers, *Z. Phys. Chem.* **3**, 497 (1889).

<sup>15</sup>L. Vegard, *Z. Physik* **5**, 17 (1921).

<sup>16</sup>W. J. L. Buyers and R. A. Cowley, in *The Fourth IAEA Symposium on Neutron Inelastic Scattering* (International Atomic Energy Agency, Vienna, 1968), Vol. 1, p. 43.

<sup>17</sup>G. Lucovsky, M. Brodsky, and E. Burstein, in *Proceedings of the International Conference on Localized Excitations in Solids* (Plenum, New York, 1966), p. 592.

<sup>18</sup>I. P. Chang and S. S. Mitra, *Phys. Rev.* **172**, 924 (1968).

<sup>19</sup>R. K. Chang, B. Lacina, and P. S. Pershan, *Phys. Rev. Lett.* **17**, 755 (1966).

<sup>20</sup>J. H. Fertel and C. H. Perry, *Phys. Rev.* **184**, 874 (1969).

<sup>21</sup>H. W. Verleur and A. S. Barker, *Phys. Rev.* **149**, 715 (1966).

<sup>22</sup>F. Matossi, *J. Chem. Phys.* **19**, 161 (1951).

<sup>23</sup>D. W. Langer, Y. S. Park, and R. N. Euwema, *Phys. Rev.* **152**, 778 (1966).

<sup>24</sup>Y. S. Chen, W. Shockley, and G. L. Pearson, *Phys. Rev.* **151**, 648 (1966).

<sup>25</sup>D. W. Taylor, *Phys. Rev.* **156**, 1017 (1967).

<sup>26</sup>R. W. Davies and J. S. Langer, *Phys. Rev.* **131**, 163 (1963).

<sup>27</sup>P. S. Pershan and W. B. Lacina, *Phys. Rev. B* **1**, 1765 (1970).

<sup>28</sup>B. D. Cullity, *Elements of X-Ray Diffraction* (Addison-Wesley, Reading, Mass., 1956).

<sup>29</sup>M. Krauzman, *Compt. Rend.* **265**, 689 (1967); **265**,

1029 (1967).

<sup>30</sup>I. M. Koldhoff, P. J. Elving, and E. B. Sandell, *Treatise on Analytical Chemistry* (Interscience, New York, 1961), Vol. 7, Pt. II, p. 402.

<sup>31</sup>M. Ahtee and O. Inkinen, *Ann. Acad. Sci. Fenn. A1*, No. 106 (1951).

<sup>32</sup>A. Guinier, *X-Ray Diffraction* (Freeman, San Francisco, 1963).

<sup>33</sup>H. Klug and L. Alexander, *X-Ray Diffraction Procedures* (Wiley, New York, 1954).

<sup>34</sup>A. Taylor, *Phil. Mag.* **31**, 339 (1941).

<sup>35</sup>J. B. Cohen (private communication).

<sup>36</sup>B. E. Warren, *Prog. Met. Phys.* **8**, 147 (1968).

<sup>37</sup>M. Krauzman, *Light Scattering Spectra of Solids*, edited by G. B. Wright (Springer-Verlag, New York, 1969), p. 109.

<sup>38</sup>J. B. Page (private communication).

<sup>39</sup>J. R. D. Copley, R. W. MacPherson, and T. Timusk, *Phys. Rev.* **182**, 965 (1969).

<sup>40</sup>R. A. Cowley, W. Cochran, B. N. Brockhouse, and

A. D. B. Woods, *Phys. Rev.* **131**, 1030 (1963).

<sup>41</sup>H. K. A. Kan, Ph.D. thesis (Cornell University, 1966) (Cornell University Materials Science Center Report No. 427) (unpublished).

<sup>42</sup>Indira R. Nair and Charles T. Walker, *Phys. Rev. B* **5**, 4101 (1972).

<sup>43</sup>G. Dolling, R. A. Cowley, C. Schittenhelm, and I. M. Thorson, *Phys. Rev.* **147**, 577 (1966).

<sup>44</sup>G. Raunio and S. Rolandson, *J. Phys. C: Solid State Phys.* **3**, 1013 (1970).

<sup>45</sup>A. Mitsuishi, U. S.—Japan Cooperative Seminar on Far Infrared Spectroscopy, Columbus, Ohio, 1965 (unpublished).

<sup>46</sup>W. Moller and R. Kaiser, *Z. Naturforsch. A* **25**, 1024 (1970).

<sup>47</sup>J. A. Harrington, R. T. Harley, and C. T. Walker, *Solid State Commun.* **9**, 683 (1971).

<sup>48</sup>R. T. Harley and C. T. Walker, *Phys. Rev. B* **2**, 2030 (1970).

PHYSICAL REVIEW B

VOLUME 7, NUMBER 6

15 MARCH 1973

## Pauli-Force Model Potential for Solids\*

Gary Simons<sup>†</sup> and Aaron N. Bloch

*Department of Chemistry, The Johns Hopkins University, Baltimore, Maryland 21218*

(Received 10 July 1972)

A model potential previously applied to molecules is adapted to the study of structural trends in solids. The potential, which has simple analytic one-electron eigenfunctions and eigenvalues, is based upon a Pauli-force concept and retains the salient features of *ab initio* pseudopotentials. The eigenvalues are of the quantum-defect form, so that treatment of the energy dependence of the potential parameter is particularly straightforward. A form factor is calculated in a local-screening approximation, and algebraic expressions for a core radius  $r_c$  and the form-factor node  $q_0$  are obtained. These expressions have transparent physical interpretations, and form the basis for a discussion of chemical trends in  $r_c$  and  $q_0$  in terms of a few simple parameters. The connection with well-known local model potentials is briefly explored.

### I. INTRODUCTION

During the past few years, the pseudopotential theory of solids has reached chemical fruition in the systematic treatments of covalency by Phillips<sup>1</sup> and of metallic cohesion and structure by Heine and co-workers.<sup>2-4</sup> Progress in the application of the method to molecules has been less rapid. Recently, however, one of us has shown<sup>5</sup> that certain trends in molecular structures are described by a simple model potential which may be understood in terms of a "Pauli force" between core and valence electrons. The potential has analytic one-electron eigenfunctions and eigenvalues, and leads naturally to useful constructs such as orbital electronegativities and comparative hybridizations.

In this paper we establish a basis for interpreting structural trends in solids in terms of this same model potential. In adding yet another model potential to the assortment already available, we are

not primarily concerned with matching the accuracy of successful calculations already in the literature; rather, we seek chemical insight into their results. From this point of view, the choice of a potential having analytic eigenfunctions and eigenvalues is especially attractive in that it circumvents much of the mathematics associated with the usual model potentials. In particular, the connection between potential parameters and atomic spectral data is algebraic, and in terms of these parameters we are able to develop simple expressions for structurally important quantities normally accessible only to numerical calculation. These new expressions lend themselves to straightforward physical interpretation. Insofar as the physical basis of our potential is different from others, such interpretation offers alternative descriptions of structural trends, and in some cases may elucidate their chemical nature more clearly. Moreover, the use of a potential which has already been ap-